AGU ADVANCING EARTH AND SPACE SCIENCES

JGR Oceans

RESEARCH ARTICLE
10.1029/2026JC024008

Key Points:
- Gravitational flow-generated tsunami experiments are compared with field data recorded during the 2019–2021 Stromboli events
- Field tsunami amplitudes are reliably predicted by a recent empirical scaling developed for experimental pyroclastic flows entering water
- Experimental and field-recorded waveforms show strong similarity, enabling the development of predictive relationships

Supporting Information:
Supporting Information may be found in the online version of this article.

Correspondence to:
R. Paris,
raphael.paris@uca.fr

Citation:
Bougouin, A., Paris, R., Vaerewyck, C., Roche, O., Lane, E. M., Lacanna, G., & Ripepe, M. (2026). Forecasting of volcanic–flow tsunamis through integrated data from laboratory experiments and the 2019–2021 Stromboli events, Italy. *Journal of Geophysical Research: Oceans*, *131*, e2026JC024008. https://doi.org/10.1029/2026JC024008

Received 10 JAN 2026
Accepted 24 APR 2026

Author Contributions:
Formal analysis: A. Bougouin
Investigation: A. Bougouin
Methodology: A. Bougouin, R. Paris, C. Vaerewyck
Resources: R. Paris, G. Lacanna, M. Ripepe
Writing – original draft: A. Bougouin
Writing – review & editing: R. Paris, C. Vaerewyck, O. Roche, E. M. Lane, G. Lacanna, M. Ripepe

Forecasting of Volcanic–Flow Tsunamis Through Integrated Data From Laboratory Experiments and the 2019–2021 Stromboli Events, Italy

A. Bougouin[1,2], R. Paris[2], C. Vaerewyck[2], O. Roche[2], E. M. Lane[3], G. Lacanna[4], and M. Ripepe[4]

[1]Dipartimento di Ingegneria Informatica, Modellistica, Elettronica e Sistemistica, Università della Calabria, Rende, Italy, [2]Laboratoire Magmas et Volcans, Université Clermont Auvergne, CNRS, IRD, OPGC, Clermont-Ferrand, France, [3]Earth Sciences New Zealand, Christchurch, New Zealand, [4]Dipartimento Scienze della Terra, Università di Firenze, Firenze, Italy

Abstract Stromboli, Italy, is a unique volcano worldwide with near-continuous eruptions monitored by a multi-sensor network. Between 2019 and 2021, three events produced pyroclastic density currents along the Sciara del Fuoco that entered the sea and generated tsunamis, providing a unique data set linking flow dynamics to tsunami generation near the source. We compare these field observations—first crest amplitude, trough and full waveform—with laboratory experiments to assess lab-to-field upscaling and predictive reliability of volcanic-flow tsunamis. Using key dimensionless parameters, we show that existing experiments overestimate relative flow mass, limiting direct scaling to Stromboli events and motivating new experiments. An empirical scaling for experimental pyroclastic flows entering water, however, predicts satisfactorily observed tsunami amplitudes. Both laboratory and field data also reveal a consistent three-wave pattern, enabling the development of predictive relationships for the trough-to-amplitude ratio of the leading wave and total waveform energy. This study marks a first step toward bridging laboratory developments with field observations, opening new paths for volcanic-tsunami hazard assessment.

Plain Language Summary Stromboli island in Italy is a unique volcano worldwide with daily moderate explosive eruptions, closely monitored by an advanced multi-sensor network. Between 2019 and 2021, three events produced fast-moving volcanic flows that reached the sea and generated small tsunamis, providing a unique field data set linking flow dynamics to tsunami generation near the source. We compare these real-world observations with current knowledge and laboratory experiments to better understand how such tsunamis form and to evaluate whether laboratory results can actually represent natural events. We find that existing experiments tend to overestimate the mass of volcanic flows, limiting direct scaling to Stromboli events and motivating new experiments. A recent laboratory model, however, matches the tsunami amplitudes observed at Stromboli. Laboratory and field data also exhibit a similar three-wave pattern, helping to develop new predictions for tsunami characteristics. By linking laboratory experiments with field observations, this study enhances the assessment of volcanic-tsunami hazards.

1. Introduction

Tsunamis of non-seismic origin represent a significant hazard to coastal populations and infrastructure, yet forecasting these events remains a major challenge (Dauxois et al., 2021). This primarily arises from the diversity of their source mechanisms (Heller et al., 2019; Løvholt et al., 2015; Paris, 2015; Schindelé et al., 2024; Wünnemann & Weiss, 2015), which are often complex, localized, generally difficult to detect, and fundamentally different from those of earthquakes. Among the mechanisms of generation, those related to volcanic eruptions (Paris, 2015; Schindelé et al., 2024) have recently received significant attention following two major events: the December 2018 tsunami triggered by a landslide during the eruption of Anak Krakatau, Indonesia (Muhari et al., 2019), and the multiple local and transoceanic tsunamis recorded during the January 2022 eruption of Hunga Tonga–Hunga Ha'apai (Carvajal et al., 2022). The Anak Krakatau event is an example of tsunamis triggered by volcanic gravitational flows—the most frequent source of volcanic tsunamis (Latter, 1981; Paris et al., 2014)—as addressed here, while a similar mechanism may also have contributed to local tsunamis during the 2022 Tonga eruption (Lynett et al., 2022; Seabrook et al., 2023).

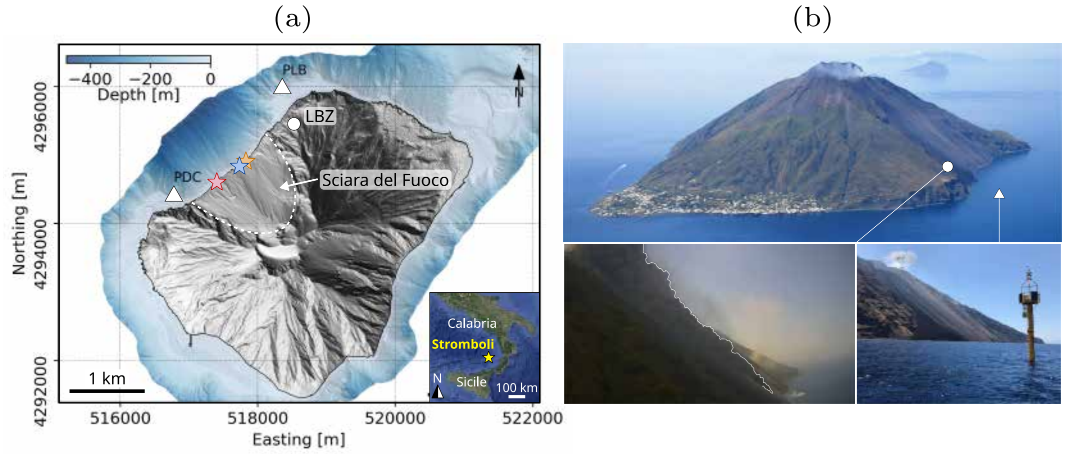

Figure 1. (a) Topography and bathymetry of Stromboli volcano showing the positions of the LBZ visible camera (circle), the wave gauges (PDC and PLB, upward triangles), and the pyroclastic-flow impacts along the Sciara del Fuoco (stars), for the events of 3 July 2019 (red), 28 August 2019 (orange), and 19 May 2021. Inset: Stromboli's location in the Tyrrhenian Sea. (b) Northeast view of Stromboli (top; photo by Carsten Steger, CC BY-SA 4.0), LBZ camera snapshot of a pyroclastic density current descending the Sciara del Fuoco on 28 August 2019 (bottom, left; LGS), and photo of the PLB wave gauge (bottom, right; LGS).

Stromboli island, located in the southern Tyrrhenian Sea, Italy, is subject to near-continuous eruptions (Rosi et al., 2000) generating regularly volcanic flows along the Sciara del Fuoco on its northwestern flank (Marsella et al., 2012; Plank et al., 2019; Ripepe & Lacanna, 2024). These flows can reach the sea, and have occasionally generated tsunamis (Giordano & De Astis, 2021; Ripepe & Lacanna, 2024). The December 2002 tsunami, triggered by a massive flank collapse of the Sciara del Fuoco, further highlights Stromboli's potential to produce substantial tsunami events and associated damage (Bonaccorso et al., 2003; Fornaciai et al., 2019; Maramai et al., 2005; Tinti et al., 2006). In such a situation, the volcanic hazard extends well beyond the island, with tsunamis potentially impacting the entire Aeolian Arc as well as the coasts of Calabria and Sicily (Figure 1). Stromboli is unique worldwide due to its advanced monitoring system, which includes a visible camera (LBZ, Figure 1) focused on the Sciara del Fuoco and two near-source wave gauges (PDC and PLB, Figure 1), as well as thermal cameras, water temperature and hydro-acoustic sensors, strainmeters and tiltmeters (Biagioli et al., 2026; Bruno et al., 2025; Ripepe & Lacanna, 2024). This monitoring system provides invaluable real-time observations of both volcanic flows and tsunamis, offering a robust field data set for assessing predictive models.

In a broader context, tsunamis generated by the impact of gravitational flows into bodies of water—such as landslides entering the ocean or rock and snow avalanches plunging into lakes—have been investigated in laboratory through idealized experiments (Bougouin et al., 2020; Bullard et al., 2019; Heller & Hager, 2010; Lipiejko et al., 2023; Miller et al., 2017; Zitti et al., 2016), numerical modeling (Battershill et al., 2021; Poulain et al., 2023; Rauter et al., 2022; Yavari-Ramshe & Ataie-Ashtiani, 2016), and theoretical analysis (Couston et al., 2015; Ma et al., 2015; Renzi & Sammarco, 2016; Walder et al., 2003; Watts & Waythomas, 2003). Nonetheless, the key physical ingredients governing tsunami generation from gravitational flows are not fully understood (Heller & Ruffini, 2023), though novel and promising research directions are currently emerging (Bougouin, Viroulet, et al., 2024; Kriaa et al., 2022; Meng & Ancey, 2019; Mulligan & Take, 2017; Sarlin et al., 2022). One approach to synthesizing results from experimental landslide-induced tsunamis have been multi-parameter regressions to develop empirical predictions (Bougouin et al., 2020; Fritz et al., 2004; Heller & Hager, 2010; Zitti et al., 2016; Zweifel et al., 2006). These predictions typically incorporate both flow characteristics (e.g., velocity, thickness, and volume) and environmental conditions (e.g., topography, water depth), expressed through dimensionless parameters to enable upscaling from the laboratory to the field. Commonly used dimensionless parameters include the Froude number $\mathcal{F}$, the relative thickness $\mathcal{H}$, and the relative mass $\mathcal{M}$, which compare the characteristic velocity, thickness and mass of the flow to those of the water body, respectively. However, the absence of a theoretical framework, the wide variety of environmental conditions not necessarily covered by the dimensionless parameters and the lack of field data—particularly data sets for both volcanic flows and associated near-field tsunamis for the same event—prevent reliable predictions.

Table 1
Dimensional and Dimensionless Field Parameters and Tsunami Amplitudes Recorded at the PDC and PLB Gauges During the 2019–2021 *Stromboli Events (Andronico et al., 2021; Ripepe & Lacanna, 2024)*

Parameters	Symbol	Unit	3 July 2019	28 August 2019	19 May 2021
Flow velocity	U_f	$m.s^{-1}$	45.6	45.7	50
Flow thickness	H_f	m	20	10	6.5
Flow Volume	V_f	m^3	2.14×10^5	1.05×10^5	0.71×10^5
Bulk flow density	D_f	$kg.m^{-3}$	380	250	368
Water depth	H_w	m	155	145	137
Froude number	$\mathcal{F}$	–	1.2	1.2	1.4
Relative thickness	$\mathcal{H}$	–	0.13	0.07	0.05
Relative mass	$\mathcal{M}$	–	0.017	0.006	0.007
Wave amplitudes	A_w^{PDC}	m	1.0	0.56[a]	0.44[a]
	A_w^{PLB}	m	0.39	0.22	0.17

[a]Fictitious Measurement Obtained by Applying the Scaling Factor $\left(A_w^{PDC}/A_w^{PLB}\right)_{3\ July}$ to the PLB Amplitudes, as the PDC Gauge was Not Operational During the Event.

With the aim to bridge the gap between laboratory studies and natural events, this work compares laboratory-based developments with field observations from the three tsunamigenic events recorded at Stromboli between 2019 and 2021. The scope is threefold: (a) to evaluate laboratory-based amplitude predictions against recent and unprecedented field observations, (b) to assess the reproducibility of field waveforms in the laboratory, and (c) to identify strengths and limitations in lab-to-field upscaling, thereby guiding for hazard assessment improvements. To achieve these goals, the paper is structured as follows. Section 2 introduces the field data set from the 2019–2021 Stromboli events. Section 3 explores lab-to-field upscaling from the Stromboli events, previous experimental studies and a new set of experiments conducted in this work. Section 4 is dedicated to the reliable assessment of laboratory-based tsunami amplitude predictions in the field, and Section 5 extends this analysis to waveform characteristics. Finally, we outline key limitations of transposing laboratory-derived insights to real-world volcanic-flow tsunami scenarios, propose guidelines to improve them, and discuss other recent—but less documented to date—tsunami events at Stromboli (Section 6).

2. The 2019–2021 Stromboli Events

Between 2019 and 2021, three tsunamigenic events were reported at Stromboli island, all triggered by pyroclastic density currents descending the steep slope of the Sciara del Fuoco ($\theta \sim 35°$) with flow fronts nearly $W_f \sim 200$ m wide, entering the sea. The flow dynamics were recorded by the video camera (LBZ, Figure 1), located on the northern side of the Sciara del Fuoco, from which nearly constant flow-front velocities along the path were estimated at $U_f \sim 45.6$ and 45.7 $m.s^{-1}$ for the 3 July and 28 August 2019 events, respectively (Ripepe & Lacanna, 2024). On 19 May 2021, lack of visibility due to an opaque ash cloud preceding the flow prevented direct velocity measurements. For this event, a front velocity of $U_f \sim 50\ m.s^{-1}$ was inferred from thermal camera observations (Calvari et al., 2022; Ripepe & Lacanna, 2024).

The side camera view also provided information on the thickness ($\sim$30 m) of the pyroclastic density currents. They consisted of two components: an upper, dilute surge that propagated over the sea surface, and a dense basal layer—referred to here and elsewhere as the pyroclastic flow—that entered the sea. Assuming that only the pyroclastic flow contributed to tsunami generation (Watts & Waythomas, 2003), both its thickness and volume were constrained from field-recorded waveforms and computational modeling. Estimated thicknesses of pyroclastic flows are $H_f = 20 \pm 4$, 10 ± 1 and 6.5 ± 1 m, and corresponding volumes are $V_f = 2.14 \pm 0.5 \times 10^5$, $1.05 \pm 0.21 \times 10^5$ and $0.71 \pm 0.15 \times 10^5\ m^3$, for the 3 July 2019, 28 August 2019 and 19 May 2021 events, respectively (Table 1; Ripepe and Lacanna (2024)). On 19 May 2021, the estimated pyroclastic flow volume agrees well with the volume of collapsed material inferred from helicopter survey photos taken immediately after the event (Calvari et al., 2022). No similar information is available for the other two events.

A last parameter useful in characterizing pyroclastic flows is the bulk flow density, which is directly related to both the mean density D_p of volcanic particles and the particle volume concentration C within the flows (Bougouin, Paris, et al., 2024). For the two 2019 paroxysms, previous studies analyzed 8–32 mm sized particle samples (Andronico et al., 2021). They provided particle density estimates that likely underestimate the average particle density of pyroclastic flows because fine ash was not considered (Eychenne & Le Pennec, 2012). They yield particle densities of $D_p \sim 760 \pm 48$ and 500 ± 118 kg.m^{-3} for the 3 July and 28 August 2019 events, respectively. No direct measurements are available for the 2021 event, but previous paroxysms in 2003, 2007 and 2019 exhibit similar particle characteristics (Andronico et al., 2021). A particle density of $D_p \sim 735 \pm 254$ kg.m^{-3} is therefore adopted for this event, based on the average of values from the four earlier paroxysms. The bulk flow density is then estimated as $D_f \sim D_p C$ with particle volume concentration $C \sim 0.5$ estimated as typical for pyroclastic flows (Delannay et al., 2017), which results in $D_f \sim 380 \pm 24$, 250 ± 59 and 368 ± 127 kg.m^{-3} for the 2019–2021 events (Table 1). Interestingly, the pyroclastic flow—the dense basal layer of a pyroclastic density current—has a density lower than that of water ($D_w \sim 10^3$ kg.m^{-3}) underlining the tsunami-generating potential of light flows entering the water, as already shown in laboratory experiments (Bougouin, Paris, et al., 2024; Zitti et al., 2016).

Within a few tens of seconds after the pyroclastic density current formed, they reached the sea and generated tsunamis. On 3 July 2019, tsunami waveforms were recorded by the two near-source wave gauges (PDC and PLB, Figure 1), but the PDC gauge ceased functioning shortly afterward due to severe damage, and was not operational during subsequent events (Ripepe & Lacanna, 2024). At the PLB gauge, the first tsunami crest amplitudes were measured as $A_w^{PLB} \sim 0.39$, 0.22, 0.17 m for the three events, while the PDC gauge recorded an amplitude of $A_w^{PDC} \sim 1.0$ m on 3 July 2019. To estimate the tsunami amplitudes at PDC for the two later events, a scaling factor based on the 3 July 2019 amplitude ratio, $\left(A_w^{PDC}/A_w^{PLB}\right)_{3\text{ July}} = 1.0/0.39 \approx 2.6$, was applied to the PLB amplitudes. This yields estimated amplitudes of $A_w^{PDC} = 0.56$ and 0.44 m for the 28 August 2019 and 19 May 2021 events, respectively.

The arrival times and locations of the wave gauges, compared with the estimated time and location of the flow impact, provided impact-to-gauge distances—approximately $R \sim 760$ m for the PDC gauge, and $R \sim 1,750$, 1,170, and 1,250 m for the PLB gauge (Figure 1)—and corresponding tsunami propagation velocities—$U_w \sim 39.0$, 37.7, and 36.7 m.s^{-1}—for the 3 July 2019, 28 August 2019, and 19 May 2021 events, respectively. The wave propagation velocity can be used to estimate the characteristic water depth H_w during tsunami generation, based on the linear shallow-water wave velocity $U_w = \sqrt{gH_w}$, where $g = 9.81$ m.s^{-2} is the gravitational acceleration (Le Méhauté, 1976). Applying this relation yields estimated characteristic water depths of $H_w = {U_w}^2/g \sim 155$, 145 and 137 m for the three events, respectively, consistent with a depth of $\sim$105 m previously reported for 3 July 2019 (Ripepe & Lacanna, 2024).

3. From Laboratory to Field: The Upscaling Challenge

When applying the laboratory results to the field, upscaling requires preserving key dimensionless parameters, namely the Froude number $\mathcal{F}$, the relative thickness $\mathcal{H}$, and the relative mass $\mathcal{M}$, defined as

$$\mathcal{F} = \frac{U_f}{\sqrt{gH_w}}, \quad \mathcal{H} = \frac{H_f}{H_w}, \quad \mathcal{M} = \frac{D_f V_f}{D_w W_f {H_w}^2}. \tag{1}$$

The relative mass can also be split as $\mathcal{M} = \mathcal{D}\mathcal{V}$, where $\mathcal{D} = D_f/D_w$ is the relative density and $\mathcal{V} = V_f/W_f {H_w}^2$ is the relative volume, which will be used separately in the following only when explicitly required.

We first assess the range of dimensionless parameters explored in laboratory experiments to date–consisting of various flowing materials descending down a slope and entering water (Bougouin et al., 2020; Bougouin, Paris, et al., 2024; Bullard et al., 2019; Heller & Hager, 2010; Lipiejko et al., 2023; Miller et al., 2017; Zitti et al., 2016)—and compare them with those from the 2019–2021 Stromboli events (Figure 2). The Froude number $\mathcal{F}$ is the most widely studied parameter in the literature due to its major influence on tsunami generation (Darvenne et al., 2024; Kriaa et al., 2022; Noda, 1970; Robbe-Saule, Morize, Bertho, et al., 2021; Robbe-Saule,

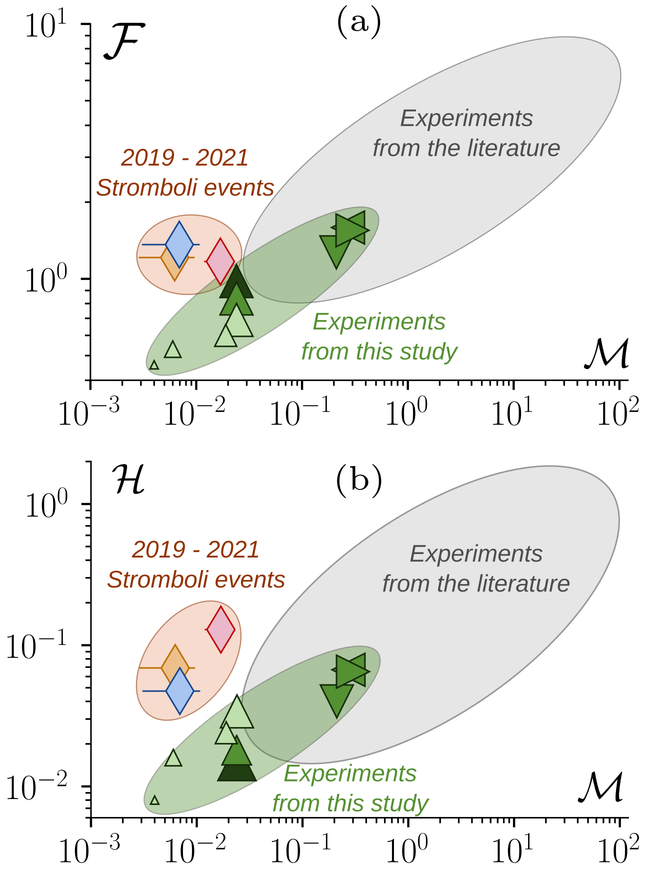

Figure 2. Range of dimensionless parameters covered by experiments from the literature (Bougouin et al., 2020; Bougouin, Paris, et al., 2024; Bullard et al., 2019; Heller & Hager, 2010; Lipiejko et al., 2023; Miller et al., 2017; Zitti et al., 2016) and from this study, as well as the 2019–2021 Stromboli events (legend detailed in Figure 4).

Morize, Henaff, et al., 2021; Sarlin et al., 2021, 2022). In laboratory experiments, the Froude number $\mathcal{F} \sim 1-10$ spans approximately one order of magnitude, encompassing the Stromboli events near the lower limit with $\mathcal{F} \sim 1.2-1.4$ (gray and orange regions, Figure 2a). A similar observation holds for the relative thickness $\mathcal{H}$, which spans two orders of magnitude in experiments ($\mathcal{H} \sim 0.01-1$), with Stromboli values of $\mathcal{H} \sim 0.05-0.13$ falling within this range (gray and orange regions, Figure 2b). In contrast, the relative mass $\mathcal{M}$ for the 2019–2021 Stromboli events lies slightly outside the wide range covered experimentally ($\mathcal{M} \sim 3 \times 10^{-2}-10^{2}$), reflecting the relatively low bulk flow densities and volumes (compared to those of water), during the Stromboli events.

To overcome the discrepancy in relative masses between published experiments and Stromboli events, we conducted new laboratory experiments in a 7 m long and 0.2 m wide channel, aimed at achieving lower values of the relative mass $\mathcal{M}$ (illustrated in Figure 4, top; see also Text S1 and Figure S1 in Supporting Information S1). The experiments consisted of the sudden release of an initially triangular-shaped mass ($M_f = 100-600$ g; bulk density, $D_f = 632$ kg.m^{-3}) of polystyrene beads (mean diameter, 140 μm; particle density, $D_p = 1050$ kg.m^{-3}) on a plane inclined at $\theta = 35°$ matching the slope of the Sciara del Fuoco. Flow velocity ($U_f = 0.85-1.82$ m.s^{-1}) and flow thickness ($H_f = 0.3-1.2$ cm) are varied through the initial mass and its position upslope of the water surface ($\Delta = 15$–76 cm; Figure S1 in Supporting Information S1). Most experiments were performed with a uniform, still water depth of $H_w = 15$ or 35 cm. However, two additional experiments include a submerged rising ramp (slope of 3° and 9°, positioned such that the maximum water depth was $H_w \sim 10$ cm; Figure S1 in Supporting Information S1) to evaluate the effect of bathymetry–reminiscent of the Sciara del Fuoco seabed from the tsunami source region to wave gauge locations. Full details of the new set of experiments are given in Supporting Information S1, and all experimental data are available in Bougouin et al. (2026).

This new set of experiments extends the existing laboratory parameter space toward lower values of $\mathcal{F}$, $\mathcal{H}$ and $\mathcal{M}$, now encompassing the range of $\mathcal{M}$ associated with the 2019–2021 Stromboli events (green and orange regions, Figure 2). However, the results emphasize the difficulty of simultaneously preserving all three dimensionless parameters—the experimental (gray and green) and field (orange) regions do not overlap—precluding full similarity between laboratory experiments and natural events. Varying the distance Δ between the initial mass and the water surface inevitably leads to both a decrease in flow thickness and an increase in velocity (Figure S1 in Supporting Information S1)—consequently a decrease in $\mathcal{H}$ and an increase in $\mathcal{F}$ (from light to dark green symbols at $\mathcal{M} \sim 2 \times 10^{-2}$, Figure 2)—in the new series of experiments. Moreover, the full set of experiments reveals clear trends between $\mathcal{M}$ and both $\mathcal{F}$ and $\mathcal{H}$ (gray and green regions, Figure 2), showing that larger released masses generally produce faster and thicker flows in the laboratory (Figure S1 in Supporting Information S1). These results underline the importance of systematically exploring a broader range of each parameter to enable robust extrapolation of empirical relationships to natural events, and emphasize that achieving full similarity between laboratory experiments and field events remains a key challenge in volcanic-flow tsunami generation—particularly at Stromboli, where natural flows appear relatively faster and thicker than those reproduced in the laboratory.

4. Laboratory-Based Tsunami Predictions in the Field

The 2019–2021 Stromboli events—remarkable for their well-documented pyroclastic density currents and near-source tsunamis (Ripepe & Lacanna, 2024)—offer a rare opportunity to evaluate laboratory-based tsunami predictions against field data. While plenty of relationships have been proposed to predict tsunami amplitudes

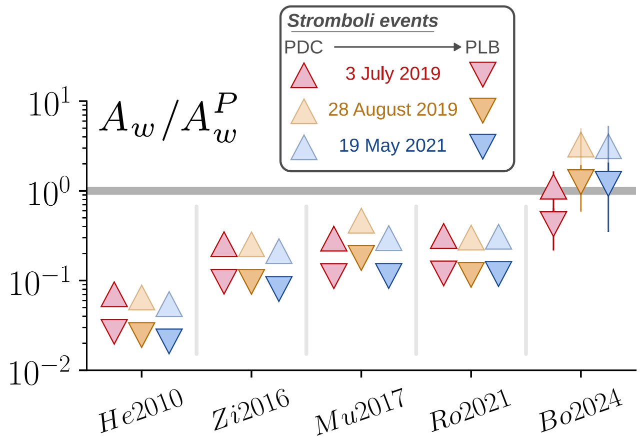

Figure 3. Tsunami amplitude A_w recorded at PDC and PLB wave gauges during the 2019–2021 Stromboli events, normalized by predicted values A_w^P from literature scalings (Equations 2–6).

based on laboratory experiments (see Heller and Ruffini (2023) and references herein), we assess here the most recent and widely used ones.

Building on several studies of impulse waves generated by a pneumatic landslide generator (Fritz et al., 2003a, 2003b, 2003c, 2004; Zweifel et al., 2006), Heller and Hager (2010) compiled a substantial number of experiments and proposed a semi-empirical relationship (hereafter denoted *He2010*) for the predicted maximum wave amplitude A_w^P as follows

$$\frac{A_w^P}{H_w} = \frac{4}{9}\left[\mathcal{F}^4\mathcal{H}^2\mathcal{M}\cos^2\left(\frac{6}{7}\theta\right)\right]^{1/5}. \quad (2)$$

Compared with Stromboli field data (Figure 3), this relationship significantly overestimates tsunami amplitudes for all three events, $A_w/A_w^P < 10^{-1}$, as recorded by the PDC and PLB wave gauges (upward and downward triangles). This discrepancy is not unique to field data, having also been reported for other laboratory experiments (Bougouin et al., 2020; Zitti et al., 2016). It has been attributed to differences in wave generation mechanisms at small and large $\mathcal{F}$ (Zitti et al., 2016), which may arise from variations in wave generation occurring above and beyond the submerged inclined ramp (Lipiejko et al., 2023). Consequently, this prediction is more appropriate for high-velocity flows in shallow water (i.e., large $\mathcal{F}$), contrasting with the 2019–2021 Stromboli events (Figure 2a and Table 1).

To fill this gap at small $\mathcal{F}$, Zitti et al. (2016) proposed an alternative empirical relationship (denoted *Zi2016*), based on impulse waves triggered by positively buoyant granular flows, as

$$\frac{A_w^P}{H_w} = 0.18\mathcal{F}^{0.0129}\mathcal{H}^{0.188}\mathcal{M}^{0.384}. \quad (3)$$

Minimizing the dependence on $\mathcal{F}$, this formulation predicts better Stromboli field data than *He2010*, though it still overpredicts tsunami amplitudes, $A_w/A_w^P \sim 0.08 - 0.25$ (Figure 3). This improvement likely reflects closer similarity in Froude number, $\mathcal{F} = 0.8 - 1.9$ and $1.2 - 1.4$, and relative flow density, $D_f/D_w \sim 0.07 - 0.25$ and $0.25 - 0.38$, between experiments and field, respectively.

Based on a theoretical framework, Mulligan and Take (2017) established two semi-analytical predictions for wave amplitude under hydrostatic and hydrodynamic conditions, which actually exhibit comparable trends. We adopt the hydrostatic formulation (denoted *Mu2017*), as applied in recent works (Bullard et al., 2019, 2023; Cabrera et al., 2020), defined as

$$\frac{A_w^P}{H_w} = \sqrt{1 + \mathcal{F}^2\mathcal{H}\mathcal{D}\cos^2\theta} - 1. \quad (4)$$

Unlike other predictions, this one excludes the relative volume $\mathcal{V}$, depending solely on $\mathcal{F}$, $\mathcal{H}$ and $\mathcal{D}$, which raises the question of whether the impacting flow can be seen as effectively infinite during the leading wave generation. Its agreement with Stromboli field data is comparable to that of *Zitti2016* (Figure 3), but it is built on theoretical arguments that offer important insights into the physical understanding of tsunami generation.

More recently, a significant advance in landslide-tsunami research has been achieved by identifying the local Froude number—based on the submerged flow velocity—as a primary control on wave amplitude (Kriaa et al., 2022; Robbe-Saule, Morize, Henaff, et al., 2021; Sarlin et al., 2021). As a direct field measurement of the submerged flow velocity is difficult, especially in field conditions, Robbe-Saule, Morize, Bertho, et al. (2021) correlated the local Froude number with the submerged flow volume, leading to the following predictive relationship (denoted *Ro2021*)

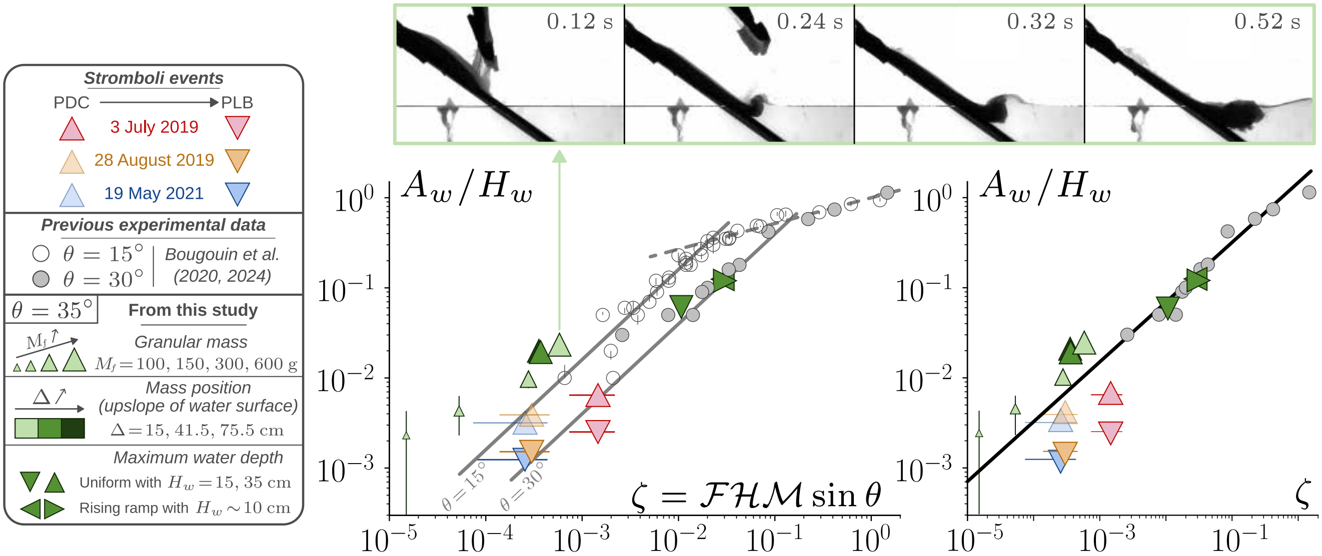

Figure 4. (Top) Successive images of a typical experiment ($M_f = 0.6$ kg, $\Delta = 15$ cm, $H_w = 35$ cm) after gate opening at $t = 0$. (Bottom, left) Normalized amplitude A_w/H_w versus dimensionless parameter $\zeta = \mathcal{FHM} \sin\theta$, for previous experiments (Bougouin et al., 2020; Bougouin, Paris, et al., 2024), the present set of experiments, and Stromboli field data. (- - -) $A_w/H_w = \zeta^{2/7}$; (—) $A_w/H_w = \alpha\zeta$ with $\alpha = 4$ and 16 for $\theta = 30°$ and 15°, respectively. (Bottom, right) Same plot excluding data with $\theta = 15°$. (—) $A_w/H_w = 1.5\zeta^{2/3}$.

$$\frac{A_w^P}{H_w} = 0.25\mathcal{V}^{0.8}. \tag{5}$$

Notably, this simplified formulation is similar to that from more complex models (*Zi2016* and *Mu2017*) in predicting tsunami amplitudes, $A_w/A_w^P \sim 0.1–0.3$, observed at Stromboli (Figure 3). Moreover, it has already shown predictive accuracy within 25% deviation for past landslide-tsunami events (Robbe-Saule, Morize, Bertho, et al., 2021), thus offering a robust and practical tool for estimating tsunami amplitudes regardless of flow and environmental complexities.

Finally, Bougouin et al. (2020) and Bougouin, Paris, et al. (2024) investigated the specific case of tsunami generation by pyroclastic flows using experimental fine-grained flows fluidized by vertical air injection prior to enter water. They identified flow volume, mass flow rate, and slope angle as determining factors, combined into a single dimensionless parameter, $\zeta = \mathcal{FHM} \sin\theta$, for predicting wave amplitudes. At low values of ζ with a slope of $\theta = 30°$—close to the conditions of the 2019–2021 Stromboli events—the resulting wave amplitude follows the empirical relation (denoted *Bo2024*)

$$\frac{A_w^P}{H_w} = 4\zeta \equiv 4\mathcal{FHM} \sin\theta. \tag{6}$$

The *Bo2024* prediction agrees well with amplitudes from the 2019–2021 Stromboli observations, regardless of the event or wave gauge, with values close to unity: $A_w^{PDC}/A_w^P \sim 1–3$ and $A_w^{PLB}/A_w^P \sim 0.4–1.3$ (Figure 3). This relationship was originally derived from wave amplitudes measured near the source, at a distance of about 10 times the water depth H_w from the impact, which is consistent with the location of the PLB gauge ($\sim 8–11H_w$) and slightly less for the PDC gauge ($\sim 5H_w$). The closer agreement may therefore stem from the fact that both *Bo2024* prediction and field observations rely on near-source amplitude measurements—rather than maximum amplitudes in other predictions—given that wave amplitudes decay during propagation.

The good agreement in predicting leading wave amplitudes from Stromboli events using the *Bo2024* scaling (Equation 6) motivates a deeper comparison including our new experimental data set (Figure 4, bottom). Prior experiments (Bougouin et al., 2020; Bougouin, Paris, et al., 2024) span wide parameter ranges—$\mathcal{F} = [0.9: 3.2]$, $\mathcal{H} = [0.015: 0.18]$, $\mathcal{M} = [0.07: 7]$, and two distinct slopes of $\theta = 15°$ and 30° (opened vs. closed circles in

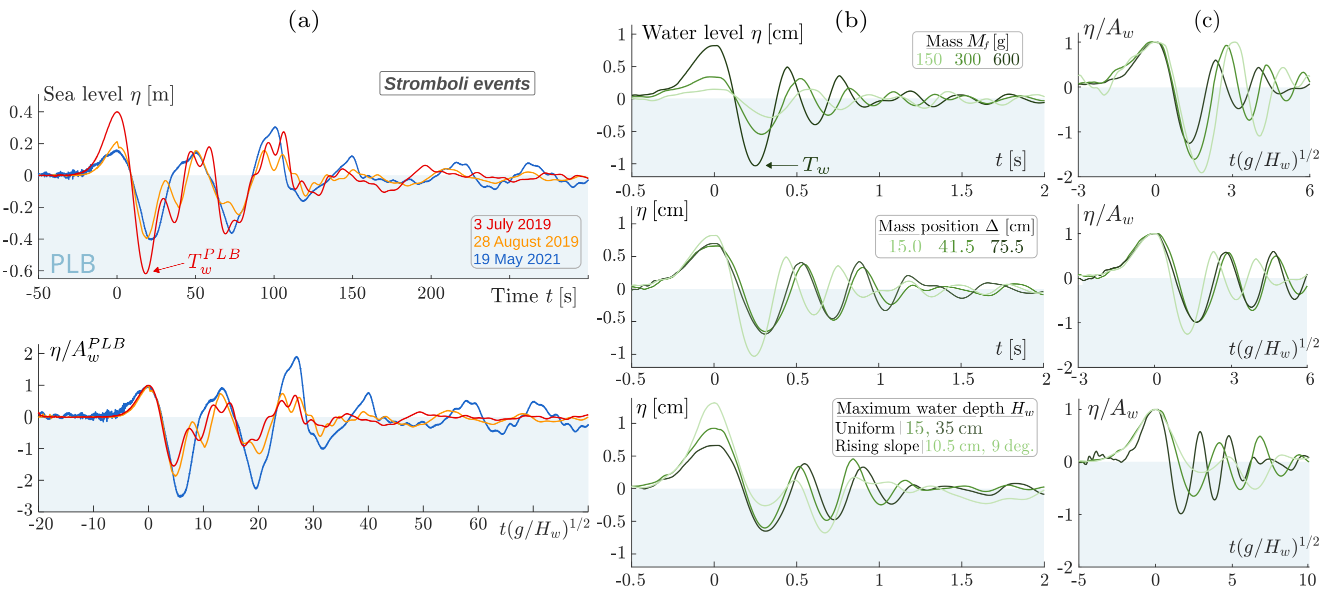

Figure 5. (a) Temporal evolution of the sea surface level η recorded at the PLB gauge during the three Stromboli events, shown in (top) dimensional and (bottom) dimensionless forms. (b, c) Temporal evolution of the water surface level η, measured at 50 cm from the shoreline, for the present experiments in (b) dimensional and (c) dimensionless forms, by varying (top) the granular mass M_f ($\Delta = 15$ cm, $H_w = 35$ cm), (middle) the initial release position Δ ($M_f = 600$ g, $H_w = 35$ cm), and (bottom) the maximum water depth H_w and associated bathymetry ($M_f = 600$ g, $\Delta = 41.5$ cm). Time origin is defined by the instant when $\eta(t = 0) = A_w$.

Figure 4, bottom left)—yielding distinct scalings. At large ζ, data collapse onto a master curve $A_w/H_w = \zeta^{2/7}$ (dashed line), accounting for θ-dependence. At low ζ—relevant to Stromboli events—A_w/H_w scales linearly with ζ, whose prefactor depends on θ (solid lines). These trends at low and high ζ likely reflect a non-breaking to breaking transition with distinct dissipation rates over distance (Bullard et al., 2019). Stromboli field data, especially from PLB gauge, are in reasonably good agreement with the $\theta = 30°$ scaling observed at low ζ (Figure 4, bottom left). In contrast, the present set of experiments (notably with $H_w = 35$ cm, upward triangles) deviate from this trend, likely due to an unappropriate water depth by using H_w, and highlights the need to better account for local bathymetry in tsunami generation. Nonetheless, our experiments enable comparison between laboratory and field data beyond wave amplitude, by examining the entire tsunami waveform as discussed below, either under $\zeta-$similarity or from data following the $\theta = 30°$ scaling. Finally, an empirical law, $A_w/H_w = 1.5\zeta^{2/3}$ (solid line in Figure 4, bottom right), also emerges from experiments with $\theta = 30 - 35°$, though it provides limited improvement in predicting field tsunami amplitudes.

5. Tsunami Waveform Comparison

To advance the lab-to-field upscaling, the entire tsunami waveforms recorded at the PLB gauge for the three events are now addressed, and then compared with those obtained from laboratory experiments.

All three field waveforms exhibit a consistent pattern of three primary tsunami waves, each characterized by a positive crest followed by a trough (Figure 5a, top). A notable difference between the events lies in the amplitude and trough of the first wave, with the largest recorded on 3 July 2019. Both the first and third waves vary across the events, whereas the intermediate wave remains relatively unchanged. By contrast, the period of each of three waves is roughly constant across all three events. On 21 May 2021, the third wave exhibits the largest amplitude within the entire waveform, suggesting a more complex or combined generation processes (e.g., successive flow events, remobilization of underwater deposits) rather than a single subaerial flow entering the sea, as it is not reproduced in laboratory experiments. Interestingly, by normalizing the sea level η by the amplitude A_w^{PLB} of the first wave and the time t by the timescale $(H_w/g)^{1/2}$ (with $t = 0$ when $\eta = A_w^{PLB}$), the first crest maintains a consistent shape across all three events (Figure 5a, bottom). However, significant differences emerge in the trough features, especially the first trough, denoted as T_w^{PLB} from now on, which will be discussed later in comparison with the experiments.

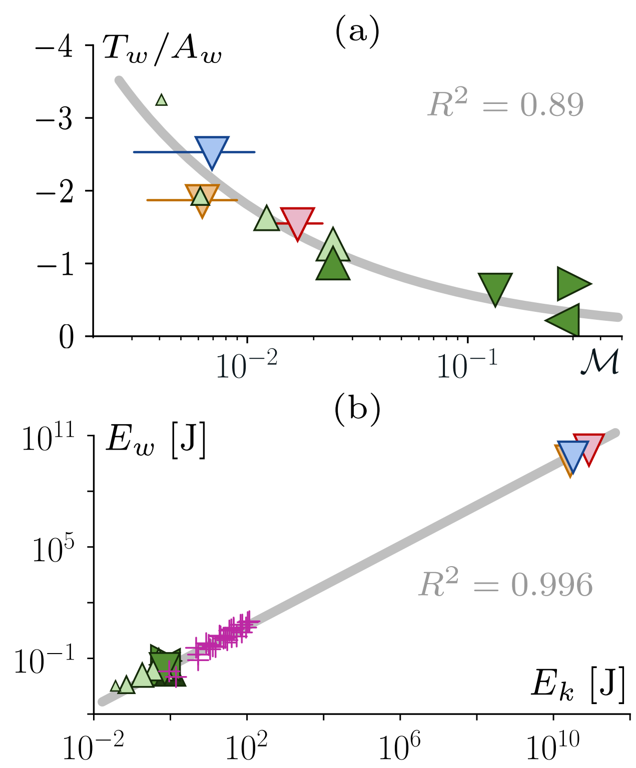

Figure 6. (a) Normalized first trough T_w/A_w versus relative mass $\mathcal{M}$, and (b) total wave energy E_w versus flow kinetic energy E_k, for the present set of experiments, Stromboli field data (see legend in Figure 4), and previous experiments (Bougouin, Paris, et al. (2024); purple plus symbols). Solid lines represent the best fits: (a) $T_w/A_w = -0.18\mathcal{M}^{-1/2}$ and (b) $E_w = 0.03E_k^{1.08}$.

As detailed in Section 3, the new set of experiments involves the sudden release of a triangular-shaped granular mass into water, for which the initial mass M_f, its initial position Δ upslope of the water surface, the maximum water depth H_w, and the associated bathymetry, were systematically varied (Figure 4, top; Text S1 and Figure S1 in Supporting Information S1). According to field observations, most experimental waveforms are characterized by three primary, well-defined waves, occasionally followed by lower-amplitude waves that are disregarded in the following (Figure 5b). All else being equal, the entrance of larger masses into water promotes larger amplitudes and shorter periods for all three successive waves (Figure 5b, top), partially consistent with field observations (Figure 5a and Table 1). As for the three field events, the normalized water level η/A_w shows good collapse of the first wave crests across experiments (Figure 5c, top), whereas the troughs remain strongly dependent on the initial mass M_f. Notably, both experimental and field data follow the scaling law $T_w/A_w = -0.18\mathcal{M}^{-1/2}$ for the first trough (Figure 6a), providing a simple manner for estimating the mass involved in tsunami generation. A similar relationship holds for the second trough, but the results are slightly more scattered (Figure S2 in Supporting Information S1). Interestingly, this finding further indicates that, for sufficiently small values of $\mathcal{M}$, the first trough can exceed the amplitude of the first crest—a behavior not previously reported, which may be attributed to the larger values of $\mathcal{M}$ considered in prior experimental studies (gray region, Figure 2).

At fixed mass and water depth, varying the initial position Δ of the granular material primarily influences the thickness and velocity of the experimental flows (Figure S1 in Supporting Information S1), but it results in moderate variations in both wave amplitude and period (Figures 5b and 5c, middle). The most pronounced difference occurs for initial positions of $\Delta = 15$ cm compared to $\Delta = 41.5$ and 71.5 cm—the granular flow being slower, but considerably thicker, than the two others (Figure S1 in Supporting Information S1). For the two latters (i.e., $\Delta = 41.5$ and 71.5 cm), however, there are only little variations in flow thickness and velocity, and similar mass flow rates, which likely explains similar wave characteristics. Since wave periods and flow velocities remain constant for field events, we hypothesize that the different period values result here from changes in flow velocity across the experiments.

The influence of water depth is investigated experimentally by varying the maximum water depth H_w in the channel and by introducing a submerged rising ramp (slope of 9°) forming a downward triangular-shaped bathymetry with a maximum depth of $H_w = 10.5$ cm (Figures 5b and 5c, bottom; Figure S1 in Supporting Information S1). In such a situation, the waveform is measured either above the horizontal bottom of the channel, or above the rising ramp. Under the same flow conditions, increasing H_w over a uniform bottom produces only moderate changes to the waveform, with a decrease in amplitude and an increase in period of the first wave (Figure 5b, bottom). However, the water depth has a pronounced effect on time normalization (Figure 5c, bottom). This suggests that the timescale $(H_w/g)^{1/2}$ is not appropriate here, as wave generation is primarily governed by local bathymetry rather than the still water depth. Further work is needed to better identify the relevant depth in such experimental settings, which is beyond the scope of the present study.

When a sloping bathymetry is introduced, the waveform is significantly altered with asymmetry and strong variations in crest and trough amplitudes relative to the uniform-depth cases (Figures 5b and 5c, bottom). These effects appear inconsistent with the field waveform patterns, suggesting that the near-source bathymetry at Stromboli does not exert a major control on tsunami waveforms though it may play a secondary role in shaping smaller-scale features within the waveform pattern.

The entire waveform also enables estimation of the total energy transferred from the granular flow to the water surface—a key parameter for tsunami hazard assessment. A fundamental difference between laboratory and field waves lies in their respective two-dimensional (2D) and three-dimensional (3D) propagation, which is expected to influence slightly wave amplitudes due to near-source measurements. However, this geometrical effect can easily be accounted for the energy estimate as

$$E_w = \beta D_w g U_w \int_0^\infty \eta^2 dt, \tag{7}$$

where $\beta = W_f$ for the 2D configuration (Bougouin, Viroulet, et al., 2024; Fritz et al., 2004; Zitti et al., 2016) and $\beta = \pi R$ for the 3D configuration (Mohammed & Fritz, 2012). Equation 7 assumes an equipartition between potential and kinetic energy, which is a satisfactory approximation for impulse waves (Bougouin, Viroulet, et al., 2024; Fritz et al., 2004; Mohammed & Fritz, 2012; Zitti et al., 2016). The total wave energy E_w is compared to the flow kinetic energy, $E_k = M_f {U_f}^2/2$, for both experiments and field events. To narrow the lab-to-field scale gap, results from past large-scale experiments of fine-grained flows entering water (Bougouin, Paris, et al., 2024) are also included into the following analysis. This extended data set shows good agreement between field and experimental results along the relationship $E_w = 0.03E_k^{1.08}$ (Figure 6b), which follows an almost-linear trend consistent with earlier findings (Zitti et al., 2016). Notably, the energy ratio E_w/E_k reaches up to 10% in laboratory according to past experimental work (Bougouin, Viroulet, et al., 2024; Clous & Abadie, 2019; Lipiejko et al., 2022; Viroulet et al., 2014; Zitti et al., 2016), whereas field observations indicate more efficient energy transfer, thus lower dissipation at impact, with values around $E_w/E_k \sim 18 - 24\%$, probably attributed to scale effects (Heller et al., 2008).

6. Discussion

6.1. Limitations and Pathways to Practical Guidelines

To date, there are inherent limitations to transposing laboratory-derived development to real-world volcanic-flow tsunami scenarios. Although all control parameters were estimated for the three Stromboli events, some of them were not measured directly and required assumptions (e.g., volume, flow thickness, density), which limits robust assessment of current modeling approaches to move toward reliable operational guidelines for monitoring and early warning.

The volume of mobilized material involved in pyroclastic density currents—critical for tsunami generation—should be more accurately constrained with remote-sensing techniques (e.g., InSAR, LiDAR), that measure pre- and post-eruption topographic changes (Arnold et al., 2016; Di Traglia et al., 2022, 2024) or from seismic data (Biagioli et al., 2026; Hibert et al., 2017). However, quantifying the volume of dense pyroclastic flows that actually contribute to tsunami generation remains challenging (Watts & Waythomas, 2003), as only part of it may contribute to the properties of the first and leading wave (Miller et al., 2017). Additionally, the representative particle density of the flow across the full grain-size distribution, which partly governs the bulk flow density, can be effectively documented through post-event field surveys (Andronico et al., 2021). Bulk flow density also depends on the volumetric concentration of particles within basal pyroclastic flows. This raises a key challenge: How can we constrain the volumetric concentration and height of natural pyroclastic flows, which are typically hidden by overlying dilute pyroclastic surges? Promising approaches lie in well-controlled laboratory experiments, where the internal structure of granular flows can be characterized through optical and acoustic methods (Breard et al., 2016; van den Wildenberg et al., 2020), together with numerical modeling that treats dense and dilute components of pyroclastic density currents separately (Kelfoun, 2017). Quantifying thermal transfers in pyroclastic density currents, which are expected to differ between dense and dilute regions, can also be envisaged to overcome this issue. Nevertheless, irrespective of the chosen approach, systematic studies are required to establish a robust parametrization linking internal properties and flow dynamics of pyroclastic density currents. In this direction, future efforts should prioritize constraining the volume and representative particle density of each event, as well as developing methods to estimate the effective height of pyroclastic flows.

An important consideration reported in lab-to-field upscaling concerns the effective water depth during tsunami generation. In the field, this depth can be inferred from tsunami propagation velocities recorded by near-field wave gauges. In laboratory experiments, however, it is commonly assumed to be the maximum water depth in the tank, which is usually appropriate when tsunami generation occurs over a distance comparable to the extent of the submerged slope. In contrast, in the present set of experiments—where small volumes were used to investigate Stromboli events—maximum amplitudes are obtained much closer to the shoreline, thus meaning that the effective water depth is less than the maximum water depth. In this way, future studies should focus on the physical role of local bathymetry in tsunami generation.

To conclude, better constraining all key impact parameters in tsunami generation, as required by the *Bo2024* prediction, through laboratory studies and field investigations of past and future events, would allow the multi-instrument monitoring system at Stromboli to serve as a primary warning tool for rapidly and easily quantifying flow conditions—and, consequently, tsunami amplitudes—and issuing early warnings. In addition, deploying similar monitoring systems at other active volcanoes would enhance warning capabilities and the real-time observations of both volcanic flows and associated tsunamis, improving greatly the assessment of predictive reliability.

6.2. Other Recent Tsunamis Recorded at Stromboli

Since the tsunamigenic events of 2019–2021, near-source wave gauges at Stromboli have recorded two additional low-amplitude tsunamis, which have been partially documented (Biagioli et al., 2026; Di Traglia et al., 2024), along with numerous other events that remain undocumented to date.

On 9 October 2022, at 07:22 UTC, an eruption produced a pyroclastic density current that traveled down the Sciara del Fuoco at $U_f = 41.6$ m.s^{-1} and entered the sea (Biagioli et al., 2026). The event triggered a very low-amplitude tsunami with a first crest, $A_w^{PDC} \equiv A_w^{PLB} \sim 2.8 \pm 0.2$ cm, followed by a trough, $T_w^{PDC} \equiv T_w^{PLB} \sim -4.5 \pm 0.1$ cm. The associated volume was initially estimated at $V_f = 6.4 \pm 1.0 \times 10^3$ m^3 from airborne topographic surveys (Di Traglia et al., 2024), and then revised upward to $V_f = 23.5 \pm 9 \times 10^3$ m^3 based on seismic signals (Biagioli et al., 2026). We assume a flow width of $W_f \sim 200$ m and a typical water depth of $H_w \sim 100$ m—based on the 2019–2021 events (Ripepe & Lacanna, 2024)—and a representative particle density of $D_p \sim 735 \pm 254$ kg.m^{-3} from previous Stromboli eruptions (Andronico et al., 2021), resulting in bulk flow density of $D_f \sim 368 \pm 127$ kg.m^{-3}. Using the *Bo2024* scaling (Equation 6), the flow height is estimated at $H_f \sim 8^{+7}_{-3}$ m and $H_f \sim 2^{+4}_{-1}$ m for the two volume estimates, consistent with values inferred for the 2019–2021 events (Table 1). In contrast, the empirical relationship based on the tsunami trough-to-amplitude ratio (Figure 6a) does not hold for this low-amplitude event: the observed ratio $T_w/A_w \sim -1.7$ would imply a volume of $V_f \sim 68^{+57}_{-26} \times 10^3$ m^3, exceeding the estimated volumes.

On 4 December 2022, at 15:19 UTC, a tsunami was generated by a pyroclastic density current impacting the sea at a high velocity of $U_f = 59.2$ m.s^{-1}, with recorded wave amplitude and trough of $A_w^{PDC} \equiv A_w^{PLB} \sim 0.4 \pm 0.05$ m and $T_w^{PDC} \equiv T_w^{PLB} \sim -0.9 \pm 0.1$ m, respectively (Biagioli et al., 2026). As for the 9 October 2022 event, two volume estimates were given—$V_f \sim 88.9 \pm 26.7 \times 10^3$ m^3 (Di Traglia et al., 2024) and $V_f \sim 80 \pm 9 \times 10^3$ m^3 (Biagioli et al., 2026)—which are comparable. Using the same assumptions as before, the *Bo2024* scaling gives a flow height of $H_f \sim 6^{+8}_{-3}$ m for both volume estimates. The observed trough-to-amplitude ratio $T_w/A_w \sim -2.3$ also provides an indirect volume estimate of $V_f = 35^{+21}_{-13} \times 10^3$ m^3, which is of the same order of magnitude but lower than the reported value.

The poor agreement between the volume estimates and predictions for the 2022 events likely results from the limited constraint on water depth, which has a significant impact on the results.

7. Conclusion

The present study aimed to bridge the gap between laboratory modeling and field observations in forecasting tsunamis generated by the entrance of volcanic flows into a water body. To this end, the data set from the three tsunamigenic events that occurred at Stromboli, Italy, between 2019 and 2021—providing detailed characterization of both pyroclastic density currents and near-source tsunamis—was analyzed in light of recent laboratory advances. Based on relevant dimensionless parameters—namely the Froude number $\mathcal{F}$, the relative thickness $\mathcal{H}$, and the relative mass $\mathcal{M}$—we showed that previous laboratory experiments do not allow for direct lab-to-field upscaling to Stromboli events, primarily due to significantly higher values of $\mathcal{M}$ in laboratory. This limitation partly reflects the scarcity of experimental studies on light flows entering the water, which—as observed at Stromboli—can also generate tsunamis. This motivated the development of a new set of experiments, consisting in the sudden release of small masses of polystyrene beads into water, designed to better replicate the field conditions.

Field tsunami amplitudes were then compared to laboratory-based predictions, highlighting the fairly good reliability of the Bougouin, Paris et al. (2024)'s scaling, albeit with deviations of up to a factor of 3. Other scaling laws remain of interest, either for the simplicity of their use (Robbe-Saule, Morize, Bertho, et al., 2021) or for their sound physical basis (Mulligan & Take, 2017). A detailed comparison of waveforms from field and experimental measurements revealed notable similarities as well as differences, emphasizing an interesting way for further investigation. A consistent pattern emerged from both experimental and field data sets, consisting of three successive waves with the first typically exhibiting the highest amplitude. Furthermore, the trough-to-amplitude ratio of the first wave was found to follow a scaling law, $T_w/A_w = -0.18\mathcal{M}^{-1/2}$, offering a promising tool to estimate the mass involved in natural tsunami generation. Finally, these results showed that the total wave energy E_w accounts for up to $\sim 10\%$ and $\sim 24\%$ of the flow kinetic energy E_k in laboratory and in the field, respectively, suggesting additional sources of dissipation at small scale. Nevertheless, the relationship $E_w = 0.03E_k^{1.08}$ provides a satisfactory prediction of the total wave energy associated with the entire wave train for both scales.

This study marks an initial step in bridging laboratory developments with field observations on active volcanoes, opening new perspectives for advancing volcanic tsunami hazard assessment. Future event recordings at Stromboli, and possibly on other sites if equipped with appropriate monitoring systems, will offer valuable opportunities to further constrain tsunami predictions by linking wave features to flow conditions, paving the way for operational systems.

Conflict of Interest

The authors declare no conflicts of interest relevant to this study.

Availability Statement

Data of this study have been archived at Bougouin et al. (2026).

Acknowledgments
This work was partially conducted within the framework of the ANR *Slide2Wave* (n°ANR-23-CE30-0052-04) project. This is contribution n°764 of ClerVolc program of the International Research Center for Disaster Sciences and Sustainable Development of the University Clermont Auvergne. A. Bougouin thanks *Le Clair Mont* for providing a welcoming environment, in which the revised manuscript was completed.

References

Andronico, D., Del Bello, E., D'Oriano, C., Landi, P., Pardini, F., Scarlato, P., et al. (2021). Uncovering the eruptive patterns of the 2019 double paroxysm eruption crisis of Stromboli volcano. *Nature Communications*, *12*(1), 4213. https://doi.org/10.1038/s41467-021-24420-1

Arnold, D. W. D., Biggs, J., Wadge, G., Ebmeier, S. K., Odbert, H. M., & Poland, M. P. (2016). Dome growth, collapse, and valley fill at Soufrière Hills Volcano, Montserrat, from 1995 to 2013: Contributions from satellite radar measurements of topographic change. *Geosphere*, *12*(4), 1300–1315. https://doi.org/10.1130/ges01291.1

Battershill, L., Whittaker, C. N., Lane, E. M., Popinet, S., White, J. D. L., Power, W. L., & Nomikou, P. (2021). Numerical simulations of a fluidized granular flow entry into water: Insights into modeling tsunami generation by pyroclastic density currents. *Journal of Geophysical Research: Solid Earth*, *126*(11), e2021JB022855. https://doi.org/10.1029/2021jb022855

Biagioli, F., Métaxian, J.-P., Stutzmann, E., Bernard, P., Lacanna, G., Mangeney, A., et al. (2026). Unraveling pyroclastic density current dynamics with multiparameter geophysical sensing. Commun. *Earth and Environment*, *7*(1), 111. https://doi.org/10.1038/s43247-025-03091-6

Bonaccorso, A., Calvari, S., Garfì, G., Lodato, L., & Patanè, D. (2003). Dynamics of the December 2002 flank failure and tsunami at Stromboli volcano inferred by volcanological and geophysical observations. *Geophysical Research Letters*, *30*(18). https://doi.org/10.1029/2003gl017702

Bougouin, A., Paris, R., & Roche, O. (2020). Impact of fluidized granular flows into water: Implications for tsunamis generated by pyroclastic flows. *Journal of Geophysical Research: Solid Earth*, *125*(5), e2019JB018954. https://doi.org/10.1029/2019jb018954

Bougouin, A., Paris, R., Roche, O., Siavelis, M., & Pawlak Courdavault, A. (2024). Tsunamis generated by pyroclastic flows: Experimental insights into the effect of the bulk flow density. *Bulletin of Volcanology*, *86*(4), 35. https://doi.org/10.1007/s00445-024-01704-0

Bougouin, A., Paris, R., Vaerewyck, C., Roche, O., Lane, E. M., Lacanna, G., & Ripepe, M. (2026). Data of forecasting of volcanic–flow tsunamis through integrated data from laboratory experiments and the 2019–2021 Stromboli events, Italy [Dataset]. *Zenodo*. https://doi.org/10.5281/zenodo.17551342

Bougouin, A., Viroulet, S., Lacaze, L., Roche, O., & Paris, R. (2024). Dry granular collapse into a liquid: Role of viscous dissipation on granular flow regimes and associated waves. *Physical Review Fluids*, *9*(12), 124302. https://doi.org/10.1103/physrevfluids.9.124302

Breard, E. C. P., Lube, G., Jones, J. R., Dufek, J., Cronin, S. J., Valentine, G. A., & Moebis, A. (2016). Coupling of turbulent and non-turbulent flow regimes within pyroclastic density currents. *Nature Geoscience*, *9*(10), 767–771. https://doi.org/10.1038/ngeo2794

Bruno, V., Di Lieto, B., Gambino, S., Mattia, M., Messina, D., Privitera, L., et al. (2025). Thirty years of ground deformation monitoring at Stromboli volcano. *Scientific Data*, *12*(1), 534. https://doi.org/10.1038/s41597-025-04850-y

Bullard, G. K., Mulligan, R. P., Carreira, A., & Take, W. A. (2019). Experimental analysis of tsunamis generated by the impact of landslides with high mobility. *Coastal Engineering*, *152*, 103538. https://doi.org/10.1016/j.coastaleng.2019.103538

Bullard, G. K., Mulligan, R. P., & Take, W. A. (2023). Landslide tsunamis: Exploring momentum transfer to waves generated by a range of materials with different mobility impacting water. *Landslides*, *20*(12), 2619–2633. https://doi.org/10.1007/s10346-023-02126-3

Cabrera, M. A., Pinzon, G., Take, W. A., & Mulligan, R. P. (2020). Wave generation across a continuum of landslide conditions from the collapse of partially submerged to fully submerged granular columns. *Journal of Geophysical Research: Oceans*, *125*(12), e2020JC016465. https://doi.org/10.1029/2020jc016465

Calvari, S., Di Traglia, F., Ganci, G., Bruno, V., Ciancitto, F., Di Lieto, B., et al. (2022). Multi-parametric study of an eruptive phase comprising unrest, major explosions, crater failure, pyroclastic density currents and lava flows: Stromboli volcano, 1 December 2020–30 June 2021. *Frontiers in Earth Science*, *10*, 899635. https://doi.org/10.3389/feart.2022.899635

Carvajal, M., Sepúlveda, I., Gubler, A., & Garreaud, R. (2022). Worldwide signature of the 2022 Tonga volcanic tsunami. *Geophysical Research Letters*, *49*(6), e2022GL098153. https://doi.org/10.1029/2022gl098153

Clous, L., & Abadie, S. (2019). Simulation of energy transfers in waves generated by granular slides. *Landslides*, *16*(9), 1663–1679. https://doi.org/10.1007/s10346-019-01180-0

Couston, L.-A., Mei, C. C., & Alam, M.-R. (2015). Landslide tsunamis in lakes. *Journal of Fluid Mechanics*, *772*, 784–804. https://doi.org/10.1017/jfm.2015.190

Darvenne, A., Viroulet, S., & Lacaze, L. (2024). Physical model of landslide-generated impulse waves: Experimental investigation of the wave-granular flow coupling. *Journal of Geophysical Research: Oceans*, *129*(9), e2024JC021145. https://doi.org/10.1029/2024jc021145

Dauxois, T., Peacock, T., Bauer, P., Caulfield, C. P., Cenedese, C., Gorlé, C., et al. (2021). Confronting grand challenges in environmental fluid mechanics. *Physical Review Fluids*, *6*(2), 020501. https://doi.org/10.1103/physrevfluids.6.020501

Delannay, R., Valance, A., Mangeney, A., Roche, O., & Richard, P. (2017). Granular and particle-laden flows: From laboratory experiments to field observations. *Journal of Physics D: Applied Physics*, *50*(5), 053001. https://doi.org/10.1088/1361-6463/50/5/053001

Di Traglia, F., Berardino, P., Borselli, L., Calabria, P., Calvari, S., Casalbore, D., et al. (2024). Generation of deposit-derived pyroclastic density currents by repeated crater rim failures at Stromboli Volcano (Italy). *Bulletin of Volcanology*, *86*(8), 69. https://doi.org/10.1007/s00445-024-01761-5

Di Traglia, F., Fornaciai, A., Casalbore, D., Favalli, M., Manzella, I., Romagnoli, C., et al. (2022). Subaerial-submarine morphological changes at Stromboli volcano (Italy) induced by the 2019–2020 eruptive activity. *Geomorphology*, *400*, 108093. https://doi.org/10.1016/j.geomorph.2021.108093

Eychenne, J., & Le Pennec, J.-L. (2012). Sigmoidal particle density distribution in a subplinian scoria fall deposit. *Bulletin of Volcanology*, *74*(10), 2243–2249. https://doi.org/10.1007/s00445-012-0671-4

Fornaciai, A., Favalli, M., & Nannipieri, L. (2019). Numerical simulation of the tsunamis generated by the Sciara del Fuoco landslides (Stromboli Island, Italy). *Scientific Reports*, *9*(1), 18542. https://doi.org/10.1038/s41598-019-54949-7

Fritz, H. M., Hager, W. H., & Minor, H.-E. (2003a). Landslide generated impulse waves. *Experiments in Fluids*, *35*(6), 505–519. https://doi.org/10.1007/s00348-003-0659-0

Fritz, H. M., Hager, W. H., & Minor, H.-E. (2003b). Landslide generated impulse waves. 1. Instantaneous flow fields. *Experiments in Fluids*, *35*(6), 505–519. https://doi.org/10.1007/s00348-003-0659-0

Fritz, H. M., Hager, W. H., & Minor, H.-E. (2003c). Landslide generated impulse waves. 2. Hydrodynamic impact craters. *Experiments in Fluids*, *35*(6), 520–532. https://doi.org/10.1007/s00348-003-0660-7

Fritz, H. M., Hager, W. H., & Minor, H.-E. (2004). Near field characteristics of landslide generated impulse waves. *Journal of Waterway, Port, Coastal, and Ocean Engineering*, *130*(6), 287–302. https://doi.org/10.1061/(asce)0733-950x(2004)130:6(287)

Giordano, G., & De Astis, G. (2021). The summer 2019 basaltic Vulcanian eruptions (paroxysms) of Stromboli. *Bulletin of Volcanology*, *83*, 1–27. https://doi.org/10.1007/s00445-020-01423-2

Heller, V., Chen, F., Brühl, M., Gabl, R., Chen, X., Wolters, G., & Fuchs, H. (2019). Large-scale experiments into the tsunamigenic potential of different iceberg calving mechanisms. *Scientific Reports*, *9*(1), 861. https://doi.org/10.1038/s41598-018-36634-3

Heller, V., & Hager, W. H. (2010). Impulse product parameter in landslide generated impulse waves. *Journal of Waterway, Port, Coastal, and Ocean Engineering*, *136*(3), 145–155. https://doi.org/10.1061/(asce)ww.1943-5460.0000037

Heller, V., Hager, W. H., & Minor, H. E. (2008). Scale effects in subaerial landslide generated impulse waves. *Experiments in Fluids*, *44*(5), 691–703. https://doi.org/10.1007/s00348-007-0427-7

Heller, V., & Ruffini, G. (2023). A critical review about generic subaerial landslide-tsunami experiments and options for a needed step change. *Earth-Science Reviews*, *242*, 104459. https://doi.org/10.1016/j.earscirev.2023.104459

Hibert, C., Mangeney, A., Grandjean, G., Peltier, A., DiMuro, A., Shapiro, N. M., et al. (2017). Spatio-temporal evolution of rockfall activity from 2007 to 2011 at the Piton de la Fournaise volcano inferred from seismic data. *Journal of Volcanology and Geothermal Research*, *333*, 36–52. https://doi.org/10.1016/j.jvolgeores.2017.01.007

Kelfoun, K. (2017). A two-layer depth-averaged model for both the dilute and the concentrated parts of pyroclastic currents. *Journal of Geophysical Research: Solid Earth*, *122*(6), 4293–4311. https://doi.org/10.1002/2017jb014013

Kriaa, Q., Viroulet, S., & Lacaze, L. (2022). Modeling of impulse waves generated by a viscous collapse in water. *Physical Review Fluids*, *7*(5), 054801. https://doi.org/10.1103/physrevfluids.7.054801

Latter, J. H. (1981). Tsunamis of volcanic origin: Summary of causes, with particular reference to Krakatoa, 1883. *Bulletin of Volcanology*, *44*(3), 467–490. https://doi.org/10.1007/bf02600578

Le Méhauté, B. (1976). *An introduction to hydrodynamics and water waves*. Springer.

Lipiejko, N., Whittaker, C. N., Lane, E. M., & Power, W. L. (2023). Wave generation by fluidized granular flows: Experimental insights into the maximum near-field wave amplitude. *Journal of Geophysical Research: Oceans*, *128*(6), e2022JC019583. https://doi.org/10.1029/2022jc019583

Lipiejko, N., Whittaker, C. N., Lane, E. M., White, J. D. L., & Power, W. L. (2022). Experimental modeling of tsunamis generated by pyroclastic density currents: The effects of particle size distribution on wave generation. *Journal of Geophysical Research: Solid Earth*, *127*(11), e2022JB024847. https://doi.org/10.1029/2022jb024847

Løvholt, F., Pedersen, G., Harbitz, C. B., Glimsdal, S., & Kim, J. (2015). On the characteristics of landslide tsunamis. *Philosophical Transactions of the Royal Society A*, *373*(2053), 20140376. https://doi.org/10.1098/rsta.2014.0376

Lynett, P., McCann, M., Zhou, Z., Renteria, W., Borrero, J., Greer, D., et al. (2022). Diverse tsunamigenesis triggered by the Hunga Tonga-Hunga Ha'apai eruption. *Nature*, *609*(7928), 728–733. https://doi.org/10.1038/s41586-022-05170-6

Ma, G., Kirby, J. T., Hsu, T.-J., & Shi, F. (2015). A two-layer granular landslide model for tsunami wave generation: Theory and computation. *Ocean Modelling*, *93*, 40–55. https://doi.org/10.1016/j.ocemod.2015.07.012

Maramai, A., Graziani, L., Alessio, G., Burrato, P., Colini, L., Cucci, L., et al. (2005). Near-and far-field survey report of the 30 December 2002 Stromboli (Southern Italy) tsunami. *Marine Geology*, *215*(1–2), 93–106. https://doi.org/10.1016/j.margeo.2004.11.009

Marsella, M., Baldi, P., Coltelli, M., & Fabris, M. (2012). The morphological evolution of the Sciara del Fuoco since 1868: Reconstructing the effusive activity at Stromboli volcano. *Bulletin of Volcanology*, *74*(1), 231–248. https://doi.org/10.1007/s00445-011-0516-6

Meng, Z., & Ancey, C. (2019). The effects of slide cohesion on impulse-wave formation. *Experiments in Fluids*, *60*(10), 1–14. https://doi.org/10.1007/s00348-019-2800-8

Miller, G. S., Andy, T. W., Mulligan, R. P., & McDougall, S. (2017). Tsunamis generated by long and thin granular landslides in a large flume. *Journal of Geophysical Research: Oceans*, *122*, 653–668.

Mohammed, F., & Fritz, H. M. (2012). Physical modeling of tsunamis generated by three-dimensional deformable granular landslides. *Journal of Geophysical Research*, *117*(C11), C00015. https://doi.org/10.1029/2011jc007850

Muhari, A., Heidarzadeh, M., Susmoro, H., Nugroho, H. D., Kriswati, E., Supartoyo, et al. (2019). The December 2018 Anak Krakatau volcano tsunami as inferred from post-tsunami field surveys and spectral analysis. *Pure and Applied Geophysics*, *176*(12), 5219–5233. https://doi.org/10.1007/s00024-019-02358-2

Mulligan, R. P., & Take, W. A. (2017). On the transfer of momentum from a granular landslide to a water wave. *Coastal Engineering*, *125*, 16–22. https://doi.org/10.1016/j.coastaleng.2017.04.001

Noda, E. (1970). Water waves generated by landslides. *Journal of the Waterways, Harbors and Coastal Engineering Division*, *96*(4), 835–855. https://doi.org/10.1061/awhcar.0000045

Paris, R. (2015). Source mechanisms of volcanic tsunamis. *Philosophical Transactions of the Royal Society A*, *373*(2053), 20140380. https://doi.org/10.1098/rsta.2014.0380

Paris, R., Switzer, A. D., Belousova, M., Belousov, A., Ontowirjo, B., Whelley, P. L., & Ulvrova, M. (2014). Volcanic tsunami: A review of source mechanisms, past events and hazards in Southeast Asia (Indonesia, Philippines, Papua New Guinea). *Natural Hazards*, *70*(1), 447–470. https://doi.org/10.1007/s11069-013-0822-8

Plank, S., Marchese, F., Filizzola, C., Pergola, N., Neri, M., Nolde, M., & Martinis, S. (2019). The July/August 2019 lava flows at the Sciara del Fuoco, Stromboli–Analysis from multi-sensor infrared satellite imagery. *Remote Sensing*, *11*(23), 2879. https://doi.org/10.3390/rs11232879

Poulain, P., Le Friant, A., Mangeney, A., Viroulet, S., Fernandez-Nieto, E., Castro Diaz, M., et al. (2023). Performance and limits of a shallow-water model for landslide-generated tsunamis: From laboratory experiments to simulations of flank collapses at Montagne Pelée (Martinique). *Geophysical Journal International*, *233*(2), 796–825. https://doi.org/10.1093/gji/ggac482

Rauter, M., Viroulet, S., Gylfadóttir, S. S., Fellin, W., & Løvholt, F. (2022). Granular porous landslide tsunami modelling–the 2014 Lake Askja flank collapse. *Nature Communications*, *13*(1), 678. https://doi.org/10.1038/s41467-022-28296-7

Renzi, E., & Sammarco, P. (2016). The hydrodynamics of landslide tsunamis: Current analytical models and future research directions. *Landslides*, *13*(6), 1369–1377. https://doi.org/10.1007/s10346-016-0680-z

Ripepe, M., & Lacanna, G. (2024). Volcano generated tsunami recorded in the near source. *Nature Communications*, *15*(1), 1802. https://doi.org/10.1038/s41467-024-45937-1

Robbe-Saule, M., Morize, C., Bertho, Y., Sauret, A., Hildenbrand, A., & Gondret, P. (2021). From laboratory experiments to geophysical tsunamis generated by subaerial landslides. *Scientific Reports*, *11*, 1–9. https://doi.org/10.1038/s41598-021-96369-6

Robbe-Saule, M., Morize, C., Henaff, R., Bertho, Y., Sauret, A., & Gondret, P. (2021). Experimental investigation of tsunami waves generated by granular collapse into water. *Journal of Fluid Mechanics*, *907*, A11. https://doi.org/10.1017/jfm.2020.807

Rosi, M., Bertagnini, A., & Landi, P. (2000). Onset of the persistent activity at Stromboli volcano (Italy). *Bulletin of Volcanology*, *62*(4–5), 294–300. https://doi.org/10.1007/s004450000098

Sarlin, W., Morize, C., Sauret, A., & Gondret, P. (2021). Nonlinear regimes of tsunami waves generated by a granular collapse. *Journal of Fluid Mechanics*, *919*, R6. https://doi.org/10.1017/jfm.2021.400

Sarlin, W., Morize, C., Sauret, A., & Gondret, P. (2022). From granular collapses to shallow water waves: A predictive model for tsunami generation. *Physical Review Fluids*, *7*(9), 094801. https://doi.org/10.1103/physrevfluids.7.094801

Schindelé, F., Kong, L., Lane, E. M., Paris, R., Ripepe, M., Titov, V., & Bailey, R. (2024). A review of tsunamis generated by volcanoes (TGV) source mechanism, modelling, monitoring and warning systems. *Pure and Applied Geophysics*, *181*(6), 1754–1792. https://doi.org/10.1007/s00024-024-03515-y

Seabrook, S., Mackay, K., Watson, S. J., Clare, M. A., Hunt, J. E., Yeo, I. A., et al. (2023). Volcaniclastic density currents explain widespread and diverse seafloor impacts of the 2022 Hunga Volcano eruption. *Nature Communications*, *14*(1), 7881. https://doi.org/10.1038/s41467-023-43607-2

Tinti, S., Maramai, A., Armigliato, A., Graziani, L., Manucci, A., Pagnoni, G., & Zaniboni, F. (2006). Observations of physical effects from tsunamis of December 30, 2002 at Stromboli volcano, southern Italy. *Bulletin of Volcanology*, *68*(5), 450–461. https://doi.org/10.1007/s00445-005-0021-x

van den Wildenberg, S., Jia, X., & Roche, O. (2020). Acoustic probing of the particle concentration in turbulent granular suspensions in air. *Scientific Reports*, *10*(1), 16544. https://doi.org/10.1038/s41598-020-73427-z

Viroulet, S., Sauret, A., & Kimmoun, O. (2014). Tsunami generated by a granular collapse down a rough inclined plane. *Europhysics Letters*, *105*(3), 34004. https://doi.org/10.1209/0295-5075/105/34004

Walder, J. S., Watts, P., Sorensen, O. E., & Janssen, K. (2003). Tsunamis generated by subaerial mass flows. *Journal of Geophysical Research*, *108*(B5), 2236. https://doi.org/10.1029/2001jb000707

Watts, P., & Waythomas, C. F. (2003). Theoretical analysis of tsunami generation by pyroclastic flows. *Journal of Geophysical Research*, *108*(B12). https://doi.org/10.1029/2002jb002265

Wünnemann, K., & Weiss, R. (2015). The meteorite impact-induced tsunami hazard. *Philosophical Transactions of the Royal Society A*, *373*(2053), 20140381. https://doi.org/10.1098/rsta.2014.0381

Yavari-Ramshe, S., & Ataie-Ashtiani, B. (2016). Numerical modeling of subaerial and submarine landslide-generated tsunami waves—recent advances and future challenges. *Landslides*, *13*(6), 1325–1368. https://doi.org/10.1007/s10346-016-0734-2

Zitti, G., Ancey, C., Postacchini, M., & Brocchini, M. (2016). Impulse waves generated by snow avalanches: Momentum and energy transfer to a water body. *Journal of Geophysical Research: Earth Surface*, *121*(12), 2399–2423. https://doi.org/10.1002/2016jf003891

Zweifel, A., Hager, H., & Minor, H.-E. (2006). Plane impulse waves in reservoirs. *Journal of Waterway Port, Coastal, and Ocean Engineering*, *132*(5), 356–368. https://doi.org/10.1061/(asce)0733-950x(2006)132:5(358)